Materials Characterization 179 (2021) 111324

Contents lists available at ScienceDirect

Materials Characterization

journal homepage: www.elsevier.com/locate/matchar

Effect of vanadium content on the microstructure and wear behavior of $Fe_{(13-x)}V_xB_7$ (x = 0–5) based hard surface alloy layers

Bülent Kılınç [a,*], Engin Kocaman [b], Şaduman Şen [c], Uğur Şen [c]

[a] Sakarya University of Applied Sciences, Machine and Metal Program, Vocational School of Arifiye, Arifiye 54580, Sakarya, Turkey
[b] Zonguldak Bulent Ecevit University, Faculty of Engineering, Department of Metallurgical and Materials Engineering, İncivez 67100, Zonguldak, Turkey
[c] Sakarya University, Faculty of Engineering, Department of Metallurgical and Materials Engineering, Esentepe Campus, 54187, Sakarya, Turkey

ARTICLE INFO

Keywords:
TIG
Hardfacing
Surface alloying
Fe-V-B alloy
Hardness
Wear

ABSTRACT

In this study, $Fe_{(13-x)}V_xB_7$ (x = 0, 1, 2, 3 and 5) based hard surface alloy layers were formed on SAE 1020 steel substrate surface by tungsten inert gas (TIG) welding method. The effects of vanadium addition on microstructure, hardness and wear rate in this coating layer were investigated using optical microscope, SEM (EDS), X-ray diffractometer, hardness and wear tests. As a result of microstructure studies and phase analysis, it was determined that the structures of alloy layers consist of α-(Fe,V), α-(Fe,V) + $(Fe,V)_2B$ eutectic, and (V,Fe)B phases. As a result of the macrohardness tests, it was found that the hardness of the alloy layers varied between 42.3 ± 1.7–57.2 ± 5.1 HRC. Moreover, the microhardness of iron and vanadium borides formed in the coating layers was found to be between 1901 ± 127–3082 ± 299 $HV_{0.01}$, respectively. As a result of the wear tests, it was observed that as the amount of vanadium added to the hard surface alloy layer increased, the wear rates decreased for all applied loads. Morover, Scanning Electron Microscopy (SEM) images of the worn surfaces showed that the wear mechanisms were adhesive, micro-abrasive and oxidative.

1. Introduction

Coatings and surface treatments are a successful approach to extend the life of machines by preventing severe wear and corrosion of work tools [1,2]. One of the most important methods of surface coating is hardfacing by welding technique [2].This method is used to increase the hardness and wear resistance of the substrate material without significant loss in ductility and toughness. In this method, an alloy is homogeneously deposited on the surface of a soft material (generally low and medium carbon steels) by various welding techniques [3]. The most common of these techniques are tungsten inert gas (TIG) [4], plasma transfer arc (PTA) [5], oxyacetylene welding (OAW), gas metal arc welding (GMAW), shielded metal arc welding (SMAW) and submerged arc welding (SAW) [6]. Among these techniques, TIG welding has an important place with advantages such as high deposition rate, high maneuverability, large-scale availability, low cost and compatibility with a wide range of materials [7–10]. In this proses, the desired powder composition and the surface of substrate material are simultaneously melted by the TIG welding process and an alloy layer is formed by solidification, which metallurgically bonded to the base material [11,12].

The elements such as vanadium and boron are added in various complex alloys (such as modified ferritic and austenitic steels) for energy industry [13]. Boron is used to increase their hardenability and vanadium is an element that forms stable borides such as VB and V_2B_3. In addition, vanadium borides such as Zr, Ti and Cr borides also have high melting temperature, high hardness and wear resistance [13,14]. According to the V-B binary phase diagram, there are six boride phases which include V_3B_2, VB, V_5B_6, V_3B_4, V_2B_3 and VB_2. Vanadium borides, which are used for surface protection elements and wear-resistant materials, are promising for use as anode material for alkaline batteries due to their extremely high discharge capacity [15,16].

Studies on the ternary Fe-V-B system were limited in the literature. In these studies, experimental and theoretical information about the system has been published [13,17,18]. Its superior properties such as high hardness and high wear resistance make the Fe-V-B system attractive for hardfacing applications. However, research on the use of this alloy system in hardfacing applications has been limited. Abakay et al. [19] produced a hard Fe-V-B based surface layer using ferro-boron, ferro-vanadium and pure iron powders on AISI 1020 steel with TIG welding method. Microstructure studies, phase analysis, hardness and wear tests of the Fe-V-B based hard surface alloy layer obtained with three different compositions in which boron is fixed at 25% atomic rate

* Corresponding author.
E-mail address: bkilinc@subu.edu.tr (B. Kılınç).

https://doi.org/10.1016/j.matchar.2021.111324
Received 6 March 2021; Received in revised form 17 June 2021; Accepted 12 July 2021
Available online 21 July 2021

were carried out. As a result of the investigations, the presence of Fe_4V, Fe_2B and VB phases in the hard alloy layer was determined and it was found that the increase in the vanadium content in the alloy composition caused an increase of the formed in the boride phases in the microstructure. In the wear test, it was observed that the increase of vanadium content in the alloy composition caused a decrease in the wear rate.

Although boride-based hard surface alloys are produced using various coating technologies, studies on vanadium boride-based hard surface alloys are limited. In this study, Fe-V-B based hard surface alloys were fabricated in various proportions by TIG welding technique. The coatings were deposited onto an SAE 1020 steel substrate. The objective of this study is to investigate the effects of vanadium content on the microstructure, hardness and wear resistance of Fe-V-B based hard surface coatings.

2. Experimental procedure

In this study, SAE 1320 steel cut to a size of 30 mm × 70 mm × 5 mm, was used as the substrate material for hard surface alloying process. The chemical composition of the steel used in the experiments, SAE 1320, was determined using the Foundry-Master Pro spectral analyzer and is given in Table 1. Applications on low carbon mild steel plates are generally preferred for hardfacing in industrial applications. For this reason, the steel plate SAE 1320 was preferred in our study. The surfaces of these plates were cleaned from oil, rust and dirt for hardfacing process.

In the experimental studies performed, ferrous boron, ferrous niobium alloys and ASC100.29 coded pure iron powder were used. Compositions of ferrous alloys and pure iron used to form boride based hard surface alloys are given in Table 2.

Ferrous alloys which were taken as a rock form was subjected to crushing, grinding and sieving processes to be less than 75 μm. Pure iron powder was only sieved. The prepared powders were determined in the composition ratios given in Table 3 to form Fe-B, Fe-V-B based hard surface alloys and mixing was carried out.

The Fe-V-B ternary phase diagram [20] was used to determine the composition ratios. The prepared powders were ground and mixed in a ball mill at 200 rpm for 2 h to ensure a homogeneous distribution of the composition. The powder to ball ratio was selected as 1/3 and 7 mm diameter steel balls were used in the mixing process. Before mixing, the containers and balls were thoroughly cleaned with pure alcohol. The powder mixtures were applied to prepared substrates with a thickness of about 2–3 mm and pressed under a pressure of 100 MPa using a hydraulic press before welding. In this way, the negativity caused by gas pressure during the TIG welding process was eliminated.

The Fe-V-B based mixture powders formed by pressing on steel substrates were melted by TIG welding method and the alloy was formed on the surface. Hardfacing with TIG welding method is a preferred method because it is economical, easy to apply and the surface quality of the coating layer is good. The coating of the hard surface alloy processes were carried out by Magmaweld ID 220 T AC/DC Pulse TIG inverter welding machine. After the process, the samples were cooled in the open atmosphere and subjected to sandblasting to remove the oxide layers and burrs formed during welding. The welding parameters applied during the process are shown in Table 4.

The specimens were prepared according to standard metallographic procedure by grinding, polishing and etching with (3%) Nital reagent. An optical microscope Nikon Epiphot 200 (OM) and a scanning electron microscope JEOL-JSM-6060 (SEM/EDS) were used for microstructural characterization of the specimens. X-ray diffraction (XRD) was performed with Rigaku XRD/D/MAX/2200/PC model X-ray diffractometer using Cu-Kα radiation. The macro hardnesses taken from the outer surfaces of the alloy layers were measured using a Bulut brand Rockwell (C scale) hardness tester by measuring in three separate areas under 150 kg load. The hardness of the phases formed in the alloyed layer, transition zone and matrix were measured under a load 0.1 N by using Future Tech FM 700 micro-hardness tester.

The surfaces of steels alloyed by the TIG welding method were prepared metallographically before the wear test. For this purpose, the alloyed surfaces were roughly polished with abrasive papers of grits 60, 120, 240, 400, 600, 800 and 1000. The wear tests of the specimens were carried out on the tribometer apparatus according to the ASTM G-99 standard. The experiments were carried out by the method Ball-On Disk using spheres of aluminum oxide (Al_2O_3) with a diameter of 10 mm and a hardness value of 2720 $HV_{0.05}$ [22]; they were carried out under 2.5 N, 5 N and 10 N load at 200 m distance and 0.1 m/s speed, 65 ± 5 humidity and 21 ± 3 °C temperature in an open atmosphere. The volume from the wear track was measured using the cross-sectional area of the wear track (A), which was determined using 3D optical microscopes (Huvitz). In the measurements, the standard deviation on the worn track was typically less than 10% of its mean value. The wear volume, V_d, was calculated using Eq. (1) [23]:

$$V_d = 2\pi rA \quad (1)$$

where r is the radius of the wear track, and A is the track cross-sectional

Table 1
Chemical composition of the substrate (wt%).

	% C	% Cr	% Mn	% Si	% P	% S	% Ni	% Mo	% Fe
Comp.	0.183	0.021	1.37	0.204	0.018	0.002	0.062	0.006	98

Table 2
Composition of used powders (wt%).

Powders	%Fe	%B	%V
Ferrous boron	82	18	–
Ferrous vanadium	33.5	–	65.5
Pure iron	99.9	–	–

Table 3
Combination rates of powders prepared for $Fe_{(13-x)}V_xB_7$ (x = 0,1,2,3 and 5) based surface alloys (at.%).

Metal alloy	Compositions	Fe	Nb	B
Fe-B based	$Fe_{13}B_7$	65	–	35
Fe-V-B based	$Fe_{12}VB_7$	60	5	35
	$Fe_{11}V_2B_7$	55	10	35
	$Fe_{10}V_3B_7$	50	15	35
	$Fe_8V_5B_7$	45	20	35

Table 4
Experimental parameters of TIG Surface alloying.

Parameter	Value
Electrode	Type WT-2 pct ThO_2
Electrode diameter	2.4 mm
Angle	70 degrees
Voltage	20 V
Current	110 A
Heat input	12.3 kJ/cm
Protective gas	Type Ar (%99.9 Ar)
Flow	12 L/min
Welding speed	0.116 cm/s

Heat input Q = η.U·I/(V.1000) (kj/cm); U: voltage (V), I: current (A), V: travel speed (cm/s), η = efficiency coefficient (η = 0.65 for the TIG method) [21].

of the worn track calculated from the profile of the wear track. Finally, the wear track formed on the disks was examined by optical microscopy, scanning electron microscopy (SEM) and energy dispersive X-ray spectroscopy (EDS).

3. Results and discussion

3.1. Microstructural and phase analysis

Fig. 1 shows the microstructure of the $Fe_8V_5B_7$ hard surface alloy with the substrate and coating layer. As a result of the microstructure investigation, it was found that the thickness of the hard coated layer was approximately 2–3 mm and had a good bonding with the substrate. It was found that this relatively thick coating layer has a smooth surface topography without porosity. In the studied microstructures, a structure consisting of three different layers such as hard surface layer, interface and substrate can be clearly seen.

SEM microstructure images of the Fe-B based alloy ($Fe_{13}B_7$) formed on the steel surface are given in Fig. 2a. Upon examination of the microstructures, it was found that eutectic (α-Fe + Fe_2B) phases were observed along with the hypereutectic primary Fe_2B massive phase.

In the study of Eroğlu [24], Fe-B based filler alloys were selected as hypoeutectic and hypereutectic alloys and the solidification structures were investigated. He found that during solidification of hypereutectic microstructures, firstly FeB (few) and the primary Fe_2B phase grow by nucleation in the liquid phase and the microstructure transformed into a eutectic (γ-Fe + Fe_2B) structure with the primary Fe_2B massive phase at 1174 °C. He explained that as the temperature decreased, the γ-Fe phase in the system transformed into martensite phase below 910 °C, and the eutectic (martensite + Fe_2B) phases/structures were formed with hypereutectic the primary Fe_2B massive phase and FeB (few). When the Fe-B phase diagram is examined [25], it is seen that solidification for hypereutectic compounds will be similar to Eroğlu's explanations. However, as a result of the analysis, no FeB and martensite phases were found in the coating layer. This is an expected situation, since the formation of these phases occurs under conditions outside the equilibrium. Morover, the x-ray diffraction pattern in Fig. 4 shows that the $Fe_{13}B_7$ based alloy consists of α-Fe and Fe_2B phases. Consequently, it can be said that the Fe-B coating layer formed on the steel surface consists of the primary Fe_2B block phase and the eutectic (α-Fe + Fe_2B) phase.

SEM microstructure images of $Fe_{(13-x)}V_xB_7$ (x = 1, 2, 3 and 5) based alloys formed on the steel surface are shown in Fig. 2b-e. As a result of the SEM investigations, it was found that the primary α-Fe was formed first in compositions in which the amount of V was 5% (at.) and 10% (at.), then the Fe_2B phase was realized in eutectic form with α-Fe. Some dissolution of vanadium was also observed in both α-Fe and Fe_2B. Homolova et al. found that iron and vanadium can substitute for each other in the metal sublattice [13]. In EDS and MAP analyzes, iron and vanadium peaks can be seen together for the corresponding phases. In this case, it would be more correct to say that the primary α-(Fe,V) and eutectic (α-(Fe,V) + $(Fe,V)_2B$) phases coexist in the microstructure for compositions with atomically 5% and 10% vanadium content. However, when the vanadium content reaches 15% and 25% atomic VB is assumed to form as the phase with the highest melting temperature in block form and then continues the formation of α-Fe and Fe_2B phases in eutectic form. Also for these compounds, the microstructure at room temperature can be said to consists of primary (Fe,V)B and eutectic (α- (Fe,V) + $(Fe,V)_2B$) phases. The Fe-V-B equilibrium diagram [20], analytical results of EDS and elemental distribution maps (Fig. 3(b-i)) support this idea. Miettinen et al. found that the increase in V content promoted formation of the VB phase in their study [18]. As a result, the amount of V was not sufficient for the formation of the (V,Fe)B phase up to 15% or it caused the microstructure change to be limited. However, with the increase in vanadium (V,Fe)B phase was primarily formed, followed by formation of the eutectic α-(Fe,V) + $(Fe,V)_2B$. However, the presence of α-(Fe,V) was also observed in some cases. However, during the coating process, the local concentration differences of the composition elements and the rapid solidification conditions increased the possibility of the presence of different phases in the system. In fact, the possibility of a V_3B_4 phase was detected in analyzes of EDS and MAP, especially in coatings with 15% and 25% Vanadium content.

SEM images EDS analysis and elemental distribution maps of $Fe_8V_5B_7$ sample are given in Fig. 3. In the EDS analysis shown in Fig. 3(b-e), it can be seen at the number 1 that the intensity of the V peak is high and that there are very few Fe and B peaks. In the EDS analysis at point number 2, it can be seen that the intensity of the Fe peak is higher than the intensity of V peak. For this reason, it is assumed that the phases at points 1 and 2 are (V,Fe) B and $(Fe,V)_2B$, respectively. However, the solubility of iron in the EDS analysis from the 4th point is higher than the solubility of the iron in the EDS analysis from the 1st point. Homolova et al. he reported that the solubility of iron in the V_3B_4 phase is much higher than in the VB phase [17]. For this reason, it is assumed that it is the $(V,Fe)_3B_4$ phase in EDS number 4. The x-ray diffraction analysis in Fig. 4 also supported this idea. For $Fe_{10}V_3B_7$ and $Fe_8V_5B_7$ compounds, it was observed that the structure consisted of α-(Fe,V) + $(Fe,V)_2B$+(V,Fe)B phases and $(V,Fe)_3B_4$ phases due to the rapid solidification conditions. It is possible to say that there are α-(Fe,V) + $(Fe,V)_2B$ phases for $Fe_{12}VB_7$ and $Fe_{11}V_2B_7$ compounds.

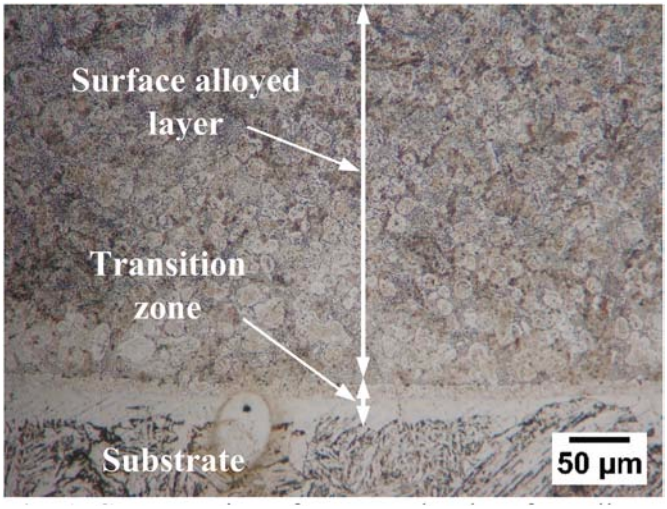

Fig. 1. Cross-section of $Fe_8V_5B_7$ hard surface alloy.

3.2. Hardness

Fig. 5 shows the measured HRC hardness values on the surfaces of the hard surface alloyed samples. As a result of the hardness measurements, HRC hardness from the surface of the Fe-B based hard surface alloy layer was determined to be 42.3 ± 1.7. The surface hardness values of Fe-V-B based hard surface alloy layers were changed between 48.3 ± 4.1–60.7 ± 3.2 HRC. The highest hardness value for this group of materials was observed composition of $Fe_8V_5B_7$. When the macro hardness curves seen in the figure are examined, it is observed that the hardness values of the alloy layer increase with the increase of vanadium. Durmuş et al. in their study found that the hardness of hard surface coatings depends largely on the proportion of primary hard phases and microstructure [26]. Gou et al. found that the hardness of the primary carbides was much higher than that of the eutectic matrix, and found that the increasing the volume fraction of the primary carbides/borides increases the hardness of the hard surface alloys [27]. A similar situation arises for the Fe-V-B based hard surface alloy system. It can be seen that with the increase of V ratio in the system, the amount of hard (Fe,V)B phase increases and the surface hardness increases in accordance with the above explanations.

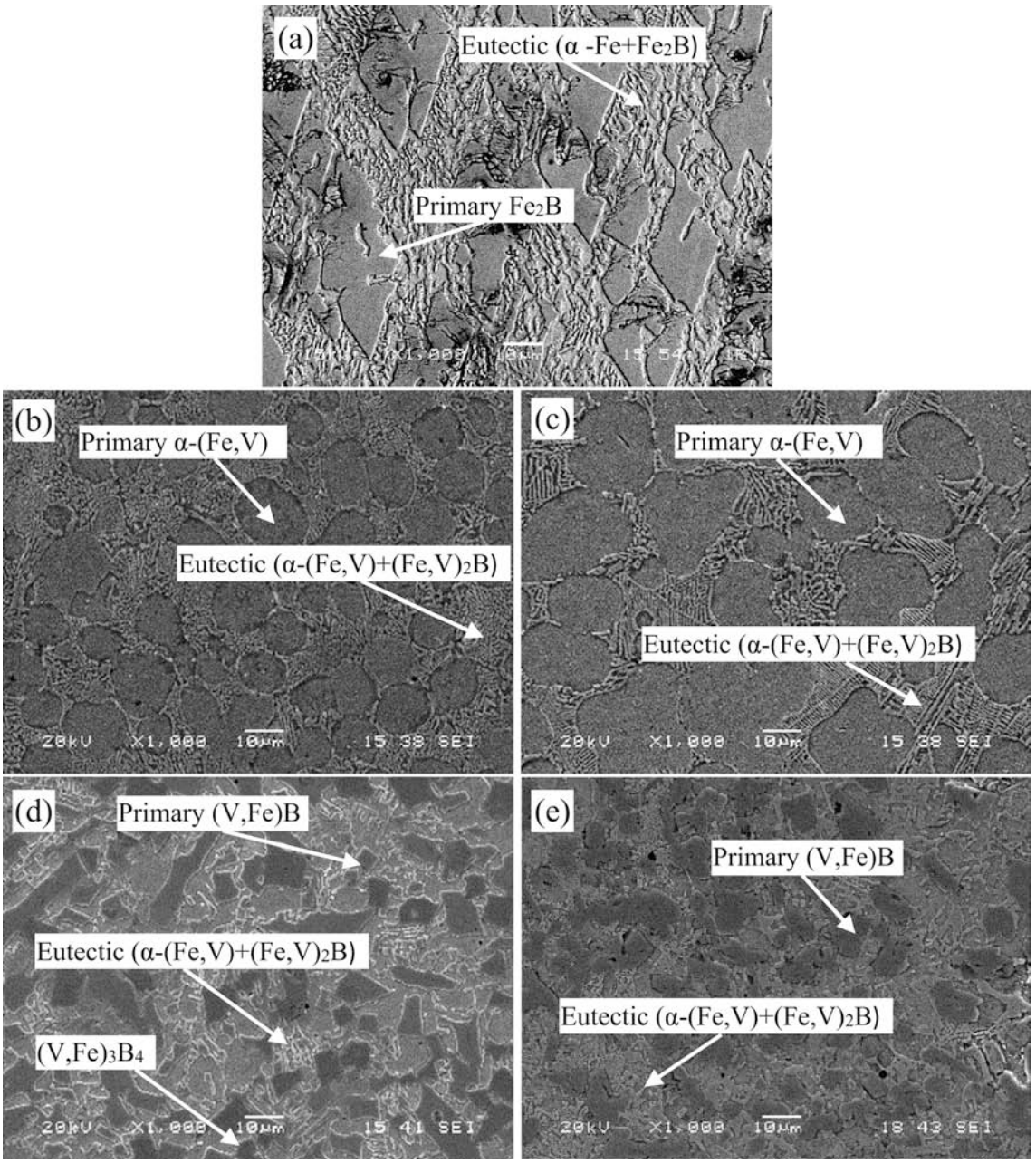

Fig. 2. SEM microstructure images of hard surface coating layers (a) $Fe_{13}B_7$ (b) $Fe_{12}VB_7$ (c) $Fe_{11}V_2B_7$ (d) $Fe_{10}V_3B_7$ (e) $Fe_8V_5B_7$.

Fig. 6 shows the phase hardness values obtained from the microhardness measurements of Fe-B, Fe-V-B based hard surface alloys. As a result of the measurements, the hardness value of the substrate (SAE 1320 steel) was found to be 185 ± 9 $HV_{0.01}$. The hardness values of the iron boride phases in the Fe-B based hard surface alloys are 1901 ± 127 $HV_{0.01}$, the hardness of the eutectic structure (α-Fe + Fe_2B) is 897 ± 82 $HV_{0.01}$ and hardness of the transition zone was found to be 369 ± 76 $HV_{0.01}$. The hardness of Fe_2B phase varies between 1100 and 2000 HV values [24,28]. The measured hardness values are in agreement with those reported in the literature.

The hardness values of the boride phases in the Fe-V-B based hard surface alloy layer vary between 2828 ± 383–3082 ± 299 $HV_{0.01}$. The highest hardness value for this phase was obtained in the $Fe_8V_5B_7$ alloy. Acording to literature review, the hardness values of vanadium boride phase vary between 2200 and 3700 HV [17]. The fact that the measured hardness value was compatible with the literature confirmed the accuracy of the findings obtained as a result of the EDS and X-ray diffraction analyzes. The hardness values of the eutectic mirostructure in the hard surface alloy layer change between 1254 ± 57–819 ± 77 $HV_{0.01}$. The hardness values of the transition zone in the hard surface alloy vary between 431 ± 27–605 ± 82 $HV_{0.01}$.

3.3. Wear behavior

The change in wear rates of Fe-B and Fe-V-B based hard surface alloy layers as a function applied load is shown in Fig. 7. Observing the wear rate curve; as given in Archard Eq. [29], the increase in load resulted in an increase in wear rate. Moreover, it can be seen that the wear rate decreases with increase in addition of V for all applied loads. The reason is believed to be that the amount boride (V and Fe) phase in the hard surface alloy layer increases. Buytoz and Eren in their study found that the increase of reinforcement content in composites decreases the values of the wear rate [30]. As stated in the microstructure explanations, it can be seen that the amount of high hardness vanadium boride phases

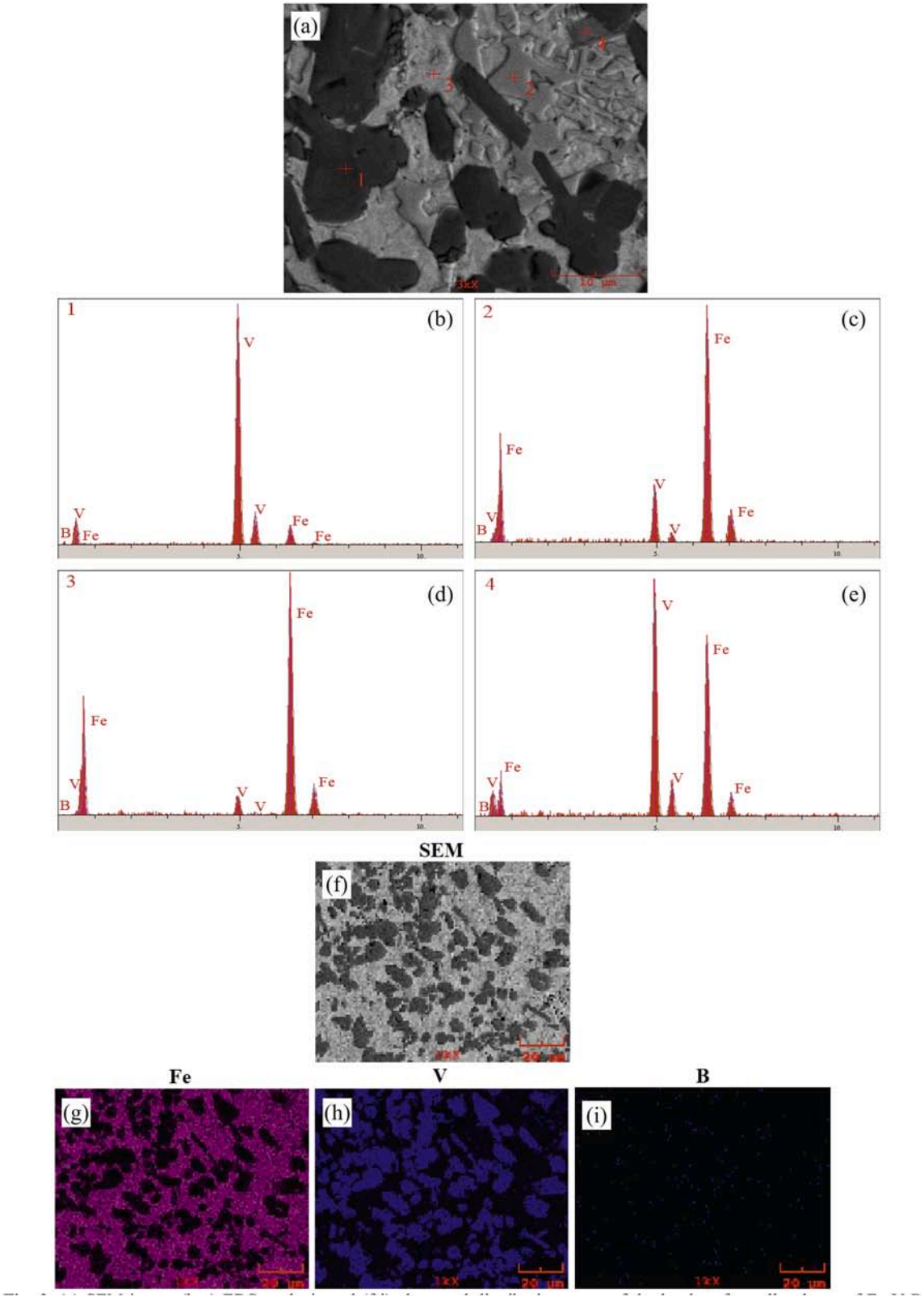

Fig. 3. (a) SEM image (b-e) EDS analysis and (f-i) elemental distribution maps of the hard surface alloy layer of $Fe_8V_5B_7$ sample.

increases due to the increase of vanadium content in the coating layer. The values obtained as a result of the hardness test clearly show that the macro hardness values of the specimens increase with the increase of V ratio. In accordance with these explanations, the wear performance of the coating layers increased with the increase of V ratio. Among the coating layers, the lowest wear rate values were obtained for $Fe_8V_5B_7$ composition for 2.5 N, 5 N and 10 N load.

While 100% increase in load (from 2.5 N to 5 N) causes 73.8% increase in wear rate for Fe-B based hard surface alloy; for 300% increase in load the increase in wear rate is 303.4%. This value causes an increase

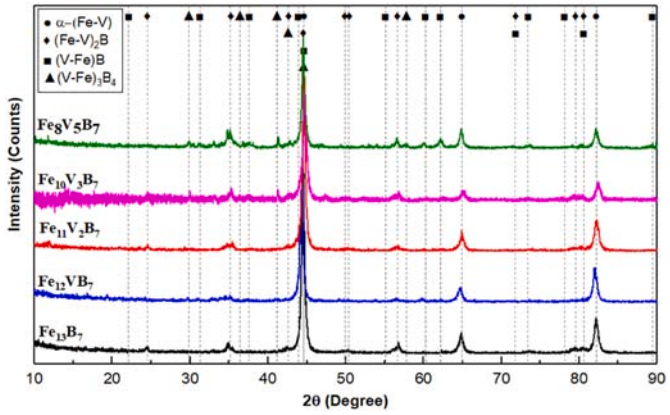

Fig. 4. X-ray diffraction pattern of Fe-V-B based hard surface alloyed steels.

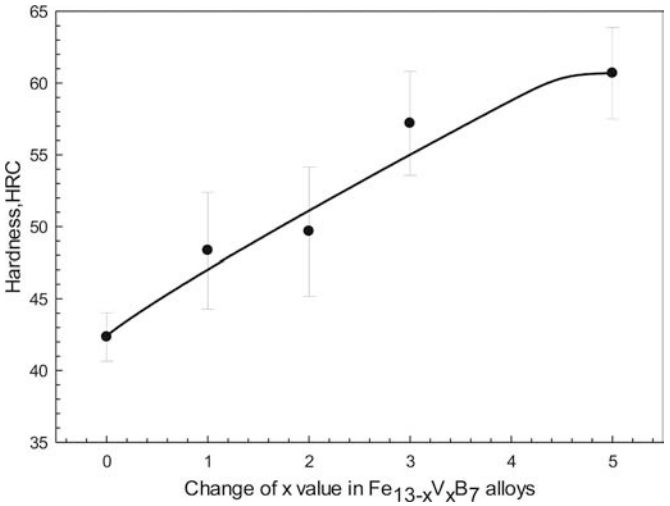

Fig. 5. Macro hardness of $Fe_{(13-x)}V_xB_7$ (x = 0, 1, 2, 3 and 5) based hard surface alloyed steels.

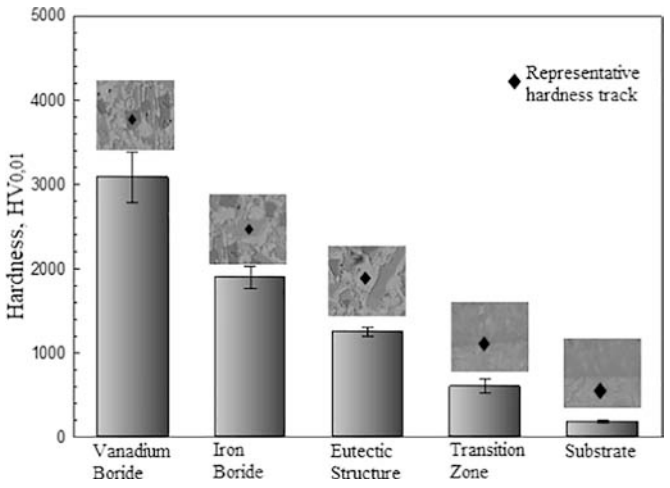

Fig. 6. Phase hardness of $Fe_{(13-x)}V_xB_7$ (x = 0, 1, 2, 3 and 5) based hard surface alloyed steels.

in wear rate for ($Fe_{(13-x)}V_xB_7$) x = 1. 2. 3 and 5 with the rates of 50–210.1%, 85.7–234.6%, 80.5–190.2% and 74.3–190% respectively, depending on the increase in V ratio. The increases in values are generally close to each other. As can be seen from the graph, the increase

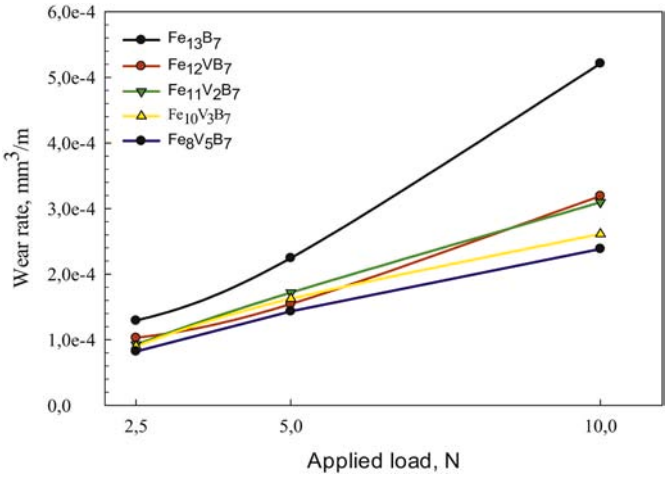

Fig. 7. Change of wear rates of Fe-B and $Fe_{(13-x)}V_xB_7$ (x = 0, 1, 2, 3 and 5) based hard surface alloy layers depending on load.

in V ratio has decreased significantly to 54.3%.

The SEM microstructure of the worn surfaces of Fe-B and Fe-V-B based hard surface alloys subjected to wear tests under 0.1 m/s and 10 N load, is shown in Fig. 8. In Fig. 8(a-b), it can be seen that the adhesive wear on the worn surface of the Fe-B based hard surface alloy layer is dominant, but there is also a small amount of abrasive wear. As a result of EDS analysis, the presence of oxides on the worn surface was found. On the worn surface of Fe-B hard surface alloy, the main wear mechanism was adhesive and oxidative wear. In addition, it could be said that there was a small abrasive wear.

SEM images of the worn surfaces of Fe-V-B based coatings are shown in Fig. 8(c-h). From these images, it can be seen that microabrasive scratches were formed on the worn surface parallel to the sliding direction. It was also possible to say that the main wear mechanism in the Fe-V-B system was adhesive wear. However, delamination wear was observed together with fatigue cracks on the worn surface of the FeV_3B_7 based coatings. In addition, worn debris was found on the surface. Fig. 9 shows the SEM image and EDS analysis of the worn surface of the $Fe_{12}VB_7$ based coating. In Fig. 9(b-d), the EDS analysis showed the presence of oxygen on the corroded surfaces. In this case, it could be said that there was oxidative wear in Fe-V-B based coatings. It was observed that hard boride phases ($(Fe,V)_2B$, (V,Fe)B and $(V,Fe)_3B_4$) increased in the microstructure with the increase of V ratio in the alloy layers and accordingly the wear track widths and wear rate decreased. In particularly, it can be seen that the region where the borides phase is present remain intact and the soft phases are eroded.

4. Conclusions

In this study, the effect of V element on microstructure and wear resistance in $Fe_{(13-x)}V_xB_7$ (x = 0, 1, 2, 3 and 5) based hard surface alloy layers was investigated. In accordance with the research and experiments, the following results were obtained:

1. The thickness of the coating layers was about 2–3 mm and showed good bonding to the substrate. In addition, a smooth surface topography without porosity was observed
2. The Fe-B base alloy ($Fe_{13}B_7$) consisted of a hyperutectic primary Fe_2B solid phase and eutectic (α-Fe + Fe_2B) phases. In compositions where the amount of V was 5% (at.) and 10% (at.), it was found that the primary α-(Fe,V) phases was formed first, followed by the eutectic $(Fe,V)_2B$+(Fe, V) phase. However, when the amount of vanadium reached the values of 15% (at.) and 25% (at.), it was found that (V, Fe)B was formed first in block form and then α-(Fe,V) + $(Fe,V)_2B$

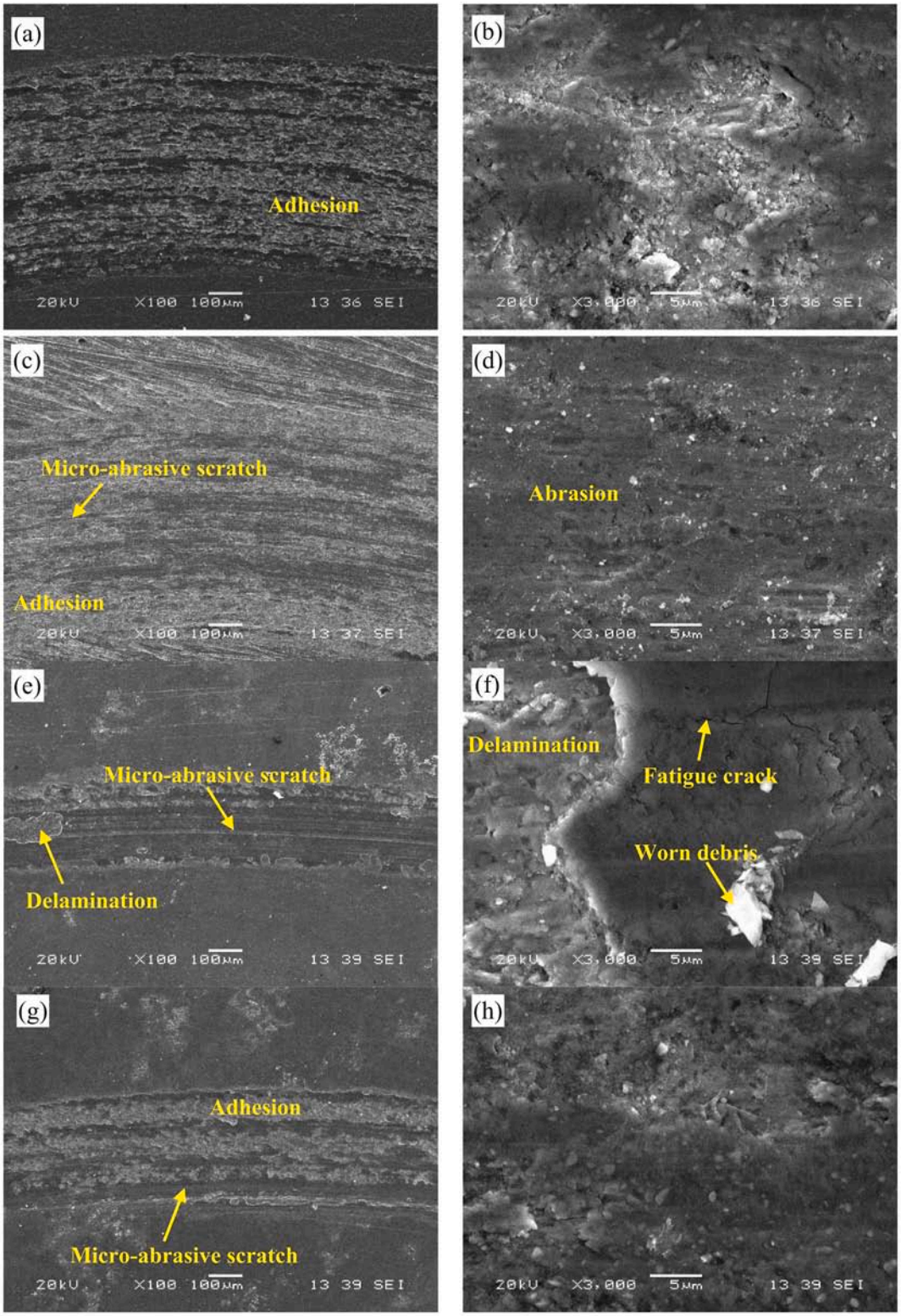

Fig. 8. The SEM micrographs of worn surfaces of samples tested at 5 N load: (a-b) $Fe_{13}B_7$ (c-d) $Fe_{12}V_2B_7$ (e-f) $Fe_{10}V_3B_7$ (g-h) $Fe_8V_5B_7$.

eutectic phases were formed. In X-ray diffraction analysis α-(Fe,V), α-$(Fe,V)_2B$, (V,Fe)B and $(V,Fe)_3B_4$ phases were determined.

3. The addition of V improved the hardness and wear resistance of Fe-V-B hard surface alloys. This indicates that the increase of vanadium, the size and volume fraction of boride particles and Fe-rich dendrites become particularly important. Among these alloys, it was found that the best wear resistance belonged to sample $Fe_8V_5B_7$. Moreover, the wear rate values of Fe $(_{13-x})V_xB_7$ (x = 0, 1, 2, 3 and 5) alloy layers were lower than the wear rate values of $Fe_{13}B_7$ hard surface alloy layer.
4. The wear test results were directly related to the hardness of the hard surface alloys. Scanning electron micrographs of the worn surfaces showed that the wear mechanisms were adhesive, micro-abrasive

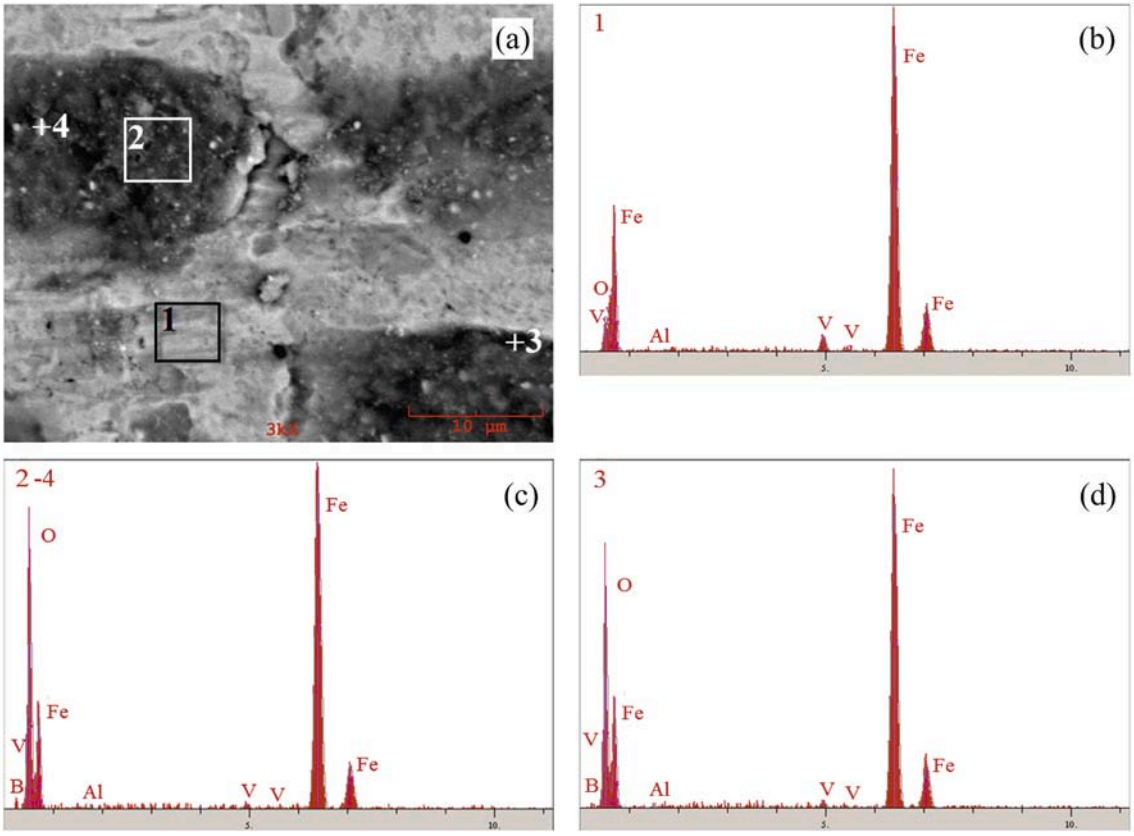

Fig. 9. (a) SEM microstructure image and (b-d) EDS analysis of $Fe_{12}VB_7$ hard surface alloy worn surface under 5 N load.

and oxidative. However, a little fatigue and delamination wear mechanisms were also found.

Declaration of Competing Interest

The authors declare that they have no known competing financial interests or personal relationships that could have appeared to influence the work reported in this paper.

Acknowledgements

The authors are grateful for the financial support from by Sakarya University Scientific Research Projects Unit with project number 2014-50-02-013.

References

[1] E. Badisch, C. Katsich, H. Winkelmann, F. Franek, M. Roy, Wear behaviour of hardfaced Fe-Cr-C alloy and austenitic steel under 2-body and 3-body conditions at elevated temperature, Tribol. Int. 43 (2010) 1234–1244, https://doi.org/10.1016/j.triboint.2010.01.008.

[2] E. Zikin, I. Badisch, C. Hussainova, H. Tomastik, Danninger, characterisation of TiC-NiMo reinforced Ni-based hardfacing, Surf. Coat. Technol. 236 (2013) 36–44, https://doi.org/10.1016/j.surfcoat.2013.02.027.

[3] M.F. Buchely, J.C. Gutierrez, L.M. Leon, A. Toro, The effect of microstructure on abrasive wear of hardfacing alloys, Wear. 259 (2005) 52–61.

[4] M.H. Korkut, O. Yilmaz, S. Buytoz, Effect of aging on the microstructure and toughness of the interface zone of a gas tungsten arc (GTA) synthesized Fe-Cr-Si-Mo-C coated low carbon steel, Surf. Coat. Technol. 157 (2002) 5–13, https://doi.org/10.1016/S0257-8972(02)00041-5.

[5] A. Zikin, I. Hussainova, C. Katsich, E. Badisch, C. Tomastik, Advanced chromium carbide-based hardfacings, Surf. Coat. Technol. 206 (2012) 4270–4278, https://doi.org/10.1016/j.surfcoat.2012.04.039.

[6] M. Kirchgaßner, E. Badisch, F. Franek, Behaviour of iron-based hardfacing alloys under abrasion and impact, Wear. 265 (2008) 772–779, https://doi.org/10.1016/j.wear.2008.01.004.

[7] K.Y. Chiu, F.T. Cheng, H.C. Man, Cavitation erosion resistance of AISI 316L stainless steel laser surface-modified with NiTi, Mater. Sci. Eng. A 392 (2005) 348–358, https://doi.org/10.1016/j.msea.2004.09.035.

[8] X.H. Wang, S.L. Song, S.Y. Qu, Z.D. Zou, Characterization of in situ synthesized TiC particle reinforced Fe-based composite coatings produced by multi-pass overlapping GTAW melting process, Surf. Coat. Technol. 201 (2007) 5899–5905, https://doi.org/10.1016/j.surfcoat.2006.10.042.

[9] Y.C. Lin, Y.H. Cho, Elucidating the microstructural and tribological characteristics of NiCrAlCoCu and NiCrAlCoMo multicomponent alloy clad layers synthesized in situ, Surf. Coat. Technol. 203 (2009) 1694–1701, https://doi.org/10.1016/j.surfcoat.2009.01.004.

[10] J.H. Chen, P.N. Chen, C.M. Lin, C.M. Chang, Y.Y. Chang, W. Wu, Characterization of multi-element alloy claddings manufactured by the tungsten inert gas process, Surf. Coat. Technol. 203 (2009) 2983–2988, https://doi.org/10.1016/j.surfcoat.2009.02.138.

[11] F. Madadi, M. Shamanian, F. Ashrafizadeh, Effect of pulse current on microstructure and wear resistance of Stellite6/tungsten carbide claddings produced by tungsten inert gas process, Surf. Coat. Technol. 205 (2011) 4320–4328, https://doi.org/10.1016/j.surfcoat.2011.03.076.

[12] B. Kilinc, O. Cegil, E. Abakay, U. Sen, S. Sen, Characterization of Fe-Nb-B base hardfacing of steel, Acta Phys. Pol. A 125 (2014) 656–658, https://doi.org/10.12693/APhysPolA.125.656.

[13] V. Homolová, A. Kroupa, A. Výrostková, Calculation of Fe-B-V ternary phase diagram, J. Alloys Compd. 520 (2012) 30–35, https://doi.org/10.1016/j.jallcom.2011.11.155.

[14] S. Sen, The characterization of vanadium boride coatings on AISI 8620 steel, Surf. Coat. Technol. 190 (2005) 1–6, https://doi.org/10.1016/j.surfcoat.2004.07.120.

[15] C.L. Yeh, H.J. Wang, Combustion synthesis of vanadium borides, J. Alloys Compd. 509 (2011) 3257–3261, https://doi.org/10.1016/j.jallcom.2010.12.004.

[16] L. Shi, Y. Gu, L. Chen, Z. Yang, J. Ma, Y. Qian, Low-temperature synthesis of nanocrystalline vanadium diboride, Mater. Lett. 58 (2004) 2890–2892, https://doi.org/10.1016/j.matlet.2004.05.013.

[17] V. Homolová, A. Výrostková, L. Ciripová, A. Kroupa, Phase analysis of Fe-B-V system, Kov. Mater. 51 (2013) 135–139, https://doi.org/10.4149/km20132135.

[18] J. Miettinen, V.V. Visuri, T. Fabritius, N. Milcheva, G. Vassilev, Thermodynamic description of ternary Fe-B-X systems. part 4: Fe-B-V, Arch. Metall. Mater. 64 (2019) 451–456, https://doi.org/10.24425/amm.2019.127559.

[19] E. Abakay, S. Sen, U. Sen, Wear properties of the surface alloyed AISI 1020 steel with vanadium and boron by TIG Welding Technique, Acta Phys. Pol. A 125 (2014) 251–253, https://doi.org/10.12693/APhysPolA.125.251.

[20] V. Raghavan, Phase Diagrams of Ternary Iron Alloys, Indian Institute of Metals, 1992.

[21] M. Ulutan, M. Yildirim, S. Buytoz, Investigation of microstructure of hardfaced AISI 4140 steel by TIG welding process, J. Eng. Archit. Fac. Eskişehir Osmangazi Univ. 12 (2009) 93–107.
[22] W. Shackelford, J.F. Alexander, Materials Science and Engineering, 3rd ed., CRC Press LLC, Washington, D.C., 2001.
[23] F. Zhou, C.M. Suh, S.S. Kim, R.I. Murakami, Sliding-wear behavior of TIN- and CrN-coated 2024 aluminum alloy against an Al2O3 ball, Tribol. Lett. 13 (2002) 173–178, https://doi.org/10.1023/A:1020103908345.
[24] M. Eroglu, Boride coatings on steel using shielded metal arc welding electrode: microstructure and hardness, Surf. Coat. Technol. 203 (2009) 2229–2235, https://doi.org/10.1016/j.surfcoat.2009.02.010.
[25] M.H. Amushahi, F. Ashrafizadeh, M. Shamanian, Characterization of boride-rich hardfacing on carbon steel by arc spray and GMAW processes, Surf. Coat. Technol. 204 (2010) 2723–2728, https://doi.org/10.1016/j.surfcoat.2010.02.028.
[26] H. Durmuş, N. Çömez, C. Gül, M. Yurddaşkal, M. Yurddaşkal, Wear performance of Fe-Cr-C-B hardfacing coatings: dry sand/rubber wheel test and ball-on-disc test, Int. J. Refract. Met. Hard Mater. 77 (2018) 37–43, https://doi.org/10.1016/j.ijrmhm.2018.07.006.
[27] J. Gou, P. Lu, Y. Wang, S. Liu, Z. Zou, Effect of nano-additives on microstructure, mechanical properties and wear behaviour of Fe-Cr-B hardfacing alloy, Appl. Surf. Sci. 360 (2016) 849–857, https://doi.org/10.1016/j.apsusc.2015.11.076.
[28] S.O. Yilmaz, M. Ozenbas, TiB2-reinforced composite coating by gas tungsten arc welding, J. Mater. Sci. 44 (2009) 3273–3284, https://doi.org/10.1007/s10853-009-3443-6.
[29] V.K. Rai, R. Srivastava, S.K. Nath, S. Ray, Wear in cast titanium carbide reinforced ferrous composites under dry sliding, Wear. 231 (1999) 265–271.
[30] S. Buytoz, H. Eren, Effect of particle reinforcements on abrasive Wear performance of aluminum metal matrix composites, Sci. Eng. J Fırat Univ. 19 (2007) 209–216.